


# Noise-induced transition from superfluid to vortex state in two-dimensional nonequilibrium polariton condensates: Semianalytical treatment

Vladimir N. Gladilin  and Michiel Wouters

*TQC, Universiteit Antwerpen, Universiteitsplein 1, B-2610 Antwerpen, Belgium*

 (Received 8 February 2023; revised 10 August 2023; accepted 2 September 2023; published 15 September 2023)

We develop a semianalytical description for the Berezinskii-Kosterlitz-Thouless–like phase transition in nonequilibrium Bose-Einstein condensates. Our theoretical analysis is based on a noisy generalized Gross-Pitaevskii equation. Above a critical strength of the noise, spontaneous vortex-antivortex pairs are generated. We provide a semianalytical determination of the transition point based on a linearized Bogoliubov analysis, to which some nonlinear corrections are added. We present two different approaches that are in agreement with our numerical calculations in a wide range of system parameters. We find that for small losses and not too small energy relaxation the critical point approaches that of the equilibrium Berezinskii-Kosterlitz-Thouless transition. Furthermore, we find that losses tend to stabilize the ordered phase: keeping the other parameters constant and increasing the losses leads to a higher critical noise strength for the spontaneous generation of vortex-antivortex pairs. Our theoretical analysis is relevant for experiments on microcavity polaritons.

DOI: [10.1103/PhysRevB.108.094510](https://doi.org/10.1103/PhysRevB.108.094510)

## I. INTRODUCTION

The interest in nonequilibrium phase transitions of quantum many body systems has witnessed a rapid growth over the last decade thanks to the developments in Bose-Einstein condensation in optical systems (microcavity polaritons and photons in dye filled cavities) [1], circuit QED [2], and ultracold atomic gases [3]. One of the most elementary phase transitions in these systems is the onset of Bose-Einstein condensation, defined as the emergence of spontaneous long range phase coherence. Where at thermal equilibrium long range phase coherence appears when the temperature is lowered below a density-dependent critical temperature, in nonequilibrium systems the phase coherence is determined by the interplay between the Hamiltonian and dissipative parts of the dynamics or even between competing dissipative mechanisms [4,5].

Since quantum fluids of light are only available in one or two dimensions, true long range order is actually absent. In one-dimensional Bose gases, both at thermal equilibrium and out of equilibrium, the spatial decay of the first order coherence function is always exponential [6,7]. In two dimensions and at equilibrium there is the celebrated Berezinskii-Kosterlitz-Thouless (BKT) phase transition [8,9] that separates the normal and the superfluid state, with exponential and algebraic decay of the spatial coherence respectively. In equilibrium, the phase dynamics is in the XY universality class and the corresponding universal jump in the superfluid stiffness has been experimentally observed in  $^4\text{He}$  [10]. More recently, the flexibility of the platform of ultracold atoms allowed a direct observation of the spontaneous formation of vortex-antivortex pairs above the BKT transition [11]. The ultracold atomic gases are in the weakly interacting regime, for which the transition temperature was computed by Prokof'ev and Svistunov by a clever combination of the linear Bogoliubov approximation and numerical Monte Carlo simulations [12].

For photonic systems out of equilibrium, the phase dynamics is actually in the Kardar-Parisi-Zhang (KPZ) universality class where a nonlinear term in the phase evolution is essential [13,14]. For one-dimensional polariton systems, the spatial decay of the correlations remains qualitatively unaffected by the nonlinearity in the phase dynamics [15], but a specific spatiotemporal scaling emerges, that was recently observed experimentally [16].

In two dimensions, the KPZ phase dynamics was predicted to make long range phase coherence impossible in isotropic systems [13,17]. Numerical studies on the other hand have shown a transition toward a state with algebraic decay of the coherence [18] and an associated disappearance of vortex-antivortex pairs [18–21] without the formation of topological defects even when the spatiotemporal correlations feature KPZ scaling [22,23]. Since computational resources limit the system sizes for numerical studies, the discrepancy between the renormalization group studies could be due to finite size effects, but at present it does not seem that the issue is fully settled. Even when the numerically observed BKT transition is due to a limited system size, experimentally available systems necessarily also work with relatively small sizes, so that there is a clear interest in the nonequilibrium BKT transition. Compared to the equilibrium case, the current understanding of the dependence of the BKT critical point on the system parameters is much less mature. The reason therefore is twofold. First, out of equilibrium the standard Boltzmann-Gibbs ensemble can no longer be used and the steady state has to be characterized by a more involved simulation of the system dynamics. Second, the nonequilibrium dynamics is governed by more parameters: in addition to the system Hamiltonian and environment temperature, also the details of the coupling to the environment come into play in the nonequilibrium situation.

In our previous work on photon condensation [24], we have pinpointed the nonequilibrium BKT critical point with

numerical simulations and developed a semianalytical approach in order to get a better understanding of the location of the critical point. In our numerical simulations, the transition was approached from the ordered side with no vortices present in the initial state. Above a critical value of the noise strength in the stochastic classical field description of the dynamics, vortex-antivortex pairs spontaneously appear, signaling the BKT-like transition to the disordered state. Our paper involved both numerical simulations and analytical approximations that capture the dependences of the transition point on all the system parameters. The analytical approximation for photon condensates was based on the Bogoliubov approximation, combined with an infrared cutoff set by the inverse vortex core size [25]. In our previous study on the BKT transition for (interacting) polaritons [20], no such analytical estimate was given.

In the present paper, we wish to fill this gap. Moreover, we extend our previous results to the regime of vanishing interactions, so that we can elucidate the effect of both the nonequilibrium condition and interactions on the BKT transition point. When the interactions become small compared to the gain saturation nonlinearity, the vortex core size can significantly deviate from the usual healing length defined as  $\xi = \hbar/\sqrt{mg\bar{n}}$ , where  $m$  is the mass,  $g$  the interaction constant, and  $\bar{n}$  the density of polaritons in the condensate. The vortex core size appears in our treatment as a good proxy for the inverse of the infrared cutoff that we have to introduce to avoid the divergence of a momentum integral. We therefore carried out a systematic analysis of the vortex size and structure as a function of the strength of the interactions and of the driving and dissipation.

The structure of this paper is as follows. In Sec. II, we introduce our model for polariton condensates and derive the density and phase fluctuations within the linear (Bogoliubov) approximation. In Sec. III, we construct some approximate formulas for the BKT critical point with a few fitting parameters that are able to capture our numerical simulations. We start with a simple approach that is able to capture the main dependencies of the critical point on the system parameters and then present a more refined approach that allows for a very good fitting of the numerical results. Conclusions are drawn in Sec. IV and the vortex structure is discussed in the Appendix.

## II. MODEL AND LINEARIZATION

We consider nonresonantly excited two-dimensional (2D) polariton condensates. In the case of sufficiently fast relaxation in the exciton reservoir, this reservoir can be adiabatically eliminated and the condensate is described by the noisy generalized Gross-Pitaevskii equation (gGPE) [26–29]:

$$(i - \kappa)\hbar \frac{\partial \psi}{\partial t} = \left[ -\frac{\hbar^2 \nabla^2}{2m} + g|\psi|^2 + \frac{i}{2} \left( \frac{P}{1 + |\psi|^2/n_s} - \gamma \right) \right] \psi + \sqrt{D}\xi. \quad (1)$$

Here  $m$  is the effective mass and the contact interaction between polaritons is characterized by the strength  $g$ . The imaginary term in the square brackets on the right hand

side describes the saturable pumping (with strength  $P$  and saturation density  $n_s$ ) that compensates for the losses ( $\gamma$ ). We take into account the energy relaxation  $\kappa$  in the condensate [30]. The complex stochastic increments have the correlation function  $\langle \xi^*(x, t)\xi(x', t') \rangle = 2\delta(\mathbf{r} - \mathbf{r}')\delta(t - t')$ . Equation (1) is a classical stochastic field model that describes all the fluctuations in the system as classical. This model is therefore only valid in the weakly interacting regime  $gm/\hbar^2 \ll 1$ , where quantum fluctuations are small.

For  $\kappa = 0$ , the zero momentum steady state of Eq. (1) is under homogeneous pumping  $\psi_0(\mathbf{x}, t) = \sqrt{n_0}e^{-ignt}$ , with  $n_0 = n_s(P/\gamma - 1)$ . By expressing the particle density  $|\psi|^2$  in units of  $n_0$ , dividing time by  $\hbar(1 + \kappa^2)/n_0$ , length by  $\hbar/\sqrt{2mn_0}$ , and noise intensity by  $\hbar^3 n_0/(2m)$ , Eq. (1) takes the form

$$\frac{\partial \psi}{\partial t} = (i + \kappa) \left[ \nabla^2 - g|\psi|^2 - \frac{i\gamma}{2n_s} \frac{1 - |\psi|^2}{1 + \nu|\psi|^2} \right] \psi + \sqrt{D}\xi, \quad (2)$$

where  $\nu = n_0/n_s$ . The steady state density is then in the absence of noise given by [20]

$$\bar{n} = \sqrt{\left( \frac{\kappa + c}{2\kappa\nu} \right)^2 + \frac{c}{\kappa\nu}} - \left( \frac{\kappa + c}{2\kappa\nu} \right) \quad (3)$$

with  $c \equiv \gamma/(2gn_s)$ .

In order to gain some insight into the physics of the fluctuations induced by the noise in Eq. (2), one can consider in first approximation the linearized equations for the density and phase fluctuations around the steady state:

$$\psi(\mathbf{x}, t) = \sqrt{\bar{n} + \delta n(\mathbf{x}, t)} e^{-ignt + i\delta\theta(\mathbf{x}, t)}. \quad (4)$$

After a spatial Fourier transform, these obey the linearized equations of motion

$$\frac{\partial}{\partial t} \delta\theta_{\mathbf{k}} = -\kappa\epsilon_{\mathbf{k}}\delta\theta_{\mathbf{k}} - \frac{\epsilon_{\mathbf{k}}}{2\bar{n}}\delta n_{\mathbf{k}} - (g - \kappa\tilde{\gamma})\delta n_{\mathbf{k}} + \sqrt{\frac{D}{\bar{n}}}\xi_{\mathbf{k}}^{(\theta)}, \quad (5)$$

$$\frac{1}{\bar{n}} \frac{\partial}{\partial t} \delta n_{\mathbf{k}} = -\kappa\epsilon_{\mathbf{k}} \frac{\delta n_{\mathbf{k}}}{\bar{n}} + 2\epsilon_{\mathbf{k}}\delta\theta_{\mathbf{k}} - 2(\kappa g + \tilde{\gamma})\delta n_{\mathbf{k}} + 2\sqrt{\frac{D}{\bar{n}}}\xi_{\mathbf{k}}^{(n)}, \quad (6)$$

where

$$\tilde{\gamma} = \frac{\gamma(1 + \nu)}{2n_s(1 + \nu\bar{n})^2}. \quad (7)$$

Using the Ito formula [31], one can obtain from Eqs. (5) and (6) a set of three equations:

$$\frac{D}{\bar{n}\epsilon_{\mathbf{k}}} = 2\kappa \langle |\delta\theta_{-\mathbf{k}}\delta n_{\mathbf{k}}|^2 \rangle + \left\langle \frac{\delta\theta_{-\mathbf{k}}\delta n_{\mathbf{k}}}{\bar{n}} \right\rangle + \frac{2(g - \kappa\tilde{\gamma})\bar{n}}{\epsilon_{\mathbf{k}}} \left\langle \frac{\delta\theta_{-\mathbf{k}}\delta n_{\mathbf{k}}}{\bar{n}} \right\rangle, \quad (8)$$

$$\frac{D}{\bar{n}\epsilon_{\mathbf{k}}} = \left[ \frac{\kappa}{2} + \frac{(\kappa g + \tilde{\gamma})\bar{n}}{\epsilon_{\mathbf{k}}} \right] \left\langle \left| \frac{\delta n_{\mathbf{k}}}{\bar{n}} \right|^2 \right\rangle - \left\langle \frac{\delta\theta_{-\mathbf{k}}\delta n_{\mathbf{k}}}{\bar{n}} \right\rangle, \quad (9)$$

$$[\epsilon_{\mathbf{k}} + 2(g - \kappa \tilde{\gamma})\bar{n}] \left\langle \left| \frac{\delta n_{\mathbf{k}}}{\bar{n}} \right|^2 \right\rangle = 4\epsilon_{\mathbf{k}} \langle |\delta\theta_{\mathbf{k}}|^2 \rangle - 4[\kappa\epsilon_{\mathbf{k}} + (\kappa g + \tilde{\gamma})\bar{n}] \left\langle \frac{\delta\theta_{-\mathbf{k}}\delta n_{\mathbf{k}}}{\bar{n}} \right\rangle, \quad (10)$$

where

$$\epsilon_{\mathbf{k}} = k^2. \quad (11)$$

Equations (8)–(10) can be solved for the density and phase fluctuations and are accurate when they are small. Close to the BKT transition, this condition however breaks down. In the following, we will outline how these equations can still be used in order to obtain an estimate for the critical point, in analogy with our study of the BKT transition in photon condensates [24].

### III. APPROXIMATIONS FOR THE BKT CRITICAL POINT

#### A. Heuristic estimate of the density-phase correlator

In order to obtain our estimate of the critical point, we start by integrating Eq. (8) over all momenta. In the right hand side, we then use that for a homogeneous system:

$$\int d^2\mathbf{k} \langle |\delta\theta_{\mathbf{k}}|^2 \rangle = \langle \delta\theta(\mathbf{x}) \delta\theta(\mathbf{x}) \rangle \equiv \langle \delta\theta^2 \rangle, \quad (12)$$

$$\int d^2\mathbf{k} \langle \delta\theta_{-\mathbf{k}}\delta n_{\mathbf{k}} \rangle = \langle \delta\theta(\mathbf{x}) \delta n(\mathbf{x}) \rangle \equiv \langle \delta\theta \delta n \rangle. \quad (13)$$

When integrating the left hand side of Eq. (8) over  $\mathbf{k}$ , we assume the presence of a finite UV momentum (energy) cutoff  $k_+$  ( $\epsilon_+ = k_+^2$ ). Our numerical simulations are performed for a lattice with grid size  $h$ , for which our UV cutoff equals  $k_+ = \pi/h$  [i.e.,  $\epsilon_+ = (\pi/h)^2$ ]. Furthermore, one has to take into account that for the systems, described by nonlinear equations similar to Eq. (2), the use of the linear approximation given by Eq. (11) is physically meaningful [12,24] only for  $k$  above a certain IR momentum (energy) cutoff  $k_-$  ( $\epsilon_- = k_-^2$ ). Then the Fourier transform of the left hand side of Eq. (8) can be represented as  $D[C_1 + \ln(\epsilon_+/\epsilon_-)]/(4\pi\bar{n})$ , where the fitting constant  $C_1$  approximates the contribution of momenta smaller than  $k_-$ .

Physically, the correlator  $\langle \delta\theta \delta n \rangle$  expresses correlations between the density and current fluctuations (since the velocity is the spatial derivative of the phase). In nonequilibrium condensates, density and velocity fluctuations are correlated because of the particle balance equation: a local suppression of the density leads to local reduction of particle losses, which is compensated by an outward flow of particles. In the context of the BKT transition, this physics plays an important role, because the density in a vortex core is reduced so that vortices are accompanied by outgoing radial currents. The magnitude of the density-phase correlator was estimated in Ref. [24] for nonequilibrium photon condensates. Following this approach, for the system under consideration here, we obtain

$$\langle \delta\theta \delta n \rangle = \frac{\tilde{\gamma}}{\bar{n}} \langle \delta N^2 \rangle, \quad (14)$$

where  $\delta N = \int_0^x \delta n(x') dx'$ . In the case of a plane density wave  $n = \bar{n}(1 - a \cos kx)$  one has

$$\langle \delta N^2 \rangle = \frac{a^2 \bar{n}^2}{2k^2}. \quad (15)$$

At the BKT transition, vortices have to nucleate, which requires in a continuum model strong density fluctuations with amplitude  $\bar{n}$  (i.e.,  $a = 1$ ) [24]. Those strong fluctuations have appreciable probability only for relatively large momenta  $k \sim k_+$  as seen from the fact that the best fitting in Ref. [24] corresponds to the effective momentum value  $k \approx 0.3k_+$  in Eq. (15). Therefore, we approximate the correlator  $\langle \delta\theta \delta n \rangle$  by  $C_2 \bar{n} \tilde{\gamma} / \epsilon_+$ , where  $C_2 \sim 1$  is a fitting parameter.

Analogously, the Fourier transform of  $\langle \delta\theta_{-\mathbf{k}} \delta n_{\mathbf{k}} \rangle / \epsilon_{\mathbf{k}}$  in the last term of Eq. (8) is approximated by  $C_3 \bar{n} \tilde{\gamma} / \epsilon_+^2$  with a fitting constant  $C_3$ . As a result, we obtain the following approximate expression for the critical noise:

$$d_{\text{BKT}} = \left\{ 2\kappa \langle \delta\theta^2 \rangle_{\text{BKT}} + \left[ C_2 + \frac{2C_3(g - \kappa \tilde{\gamma})}{\epsilon_+} \right] \frac{\tilde{\gamma}}{\epsilon_+} \right\} \times \frac{4\pi}{C_1 + \ln(\epsilon_+/\epsilon_-)}, \quad (16)$$

where  $d_{\text{BKT}} \equiv (D/\bar{n})|_{\text{BKT}}$ .

In line with Refs. [12,24], we will assume that at the transition  $\langle \delta\theta^2 \rangle_{\text{BKT}} = 1/2$ . In the equilibrium case (and at  $\kappa^2 \ll 1$ ) the IR momentum cutoff is inversely proportional to the healing length, so that the corresponding energy cutoff is  $\sim g\bar{n}$ . Since the healing length corresponds at equilibrium to the vortex core size, a natural generalization to the nonequilibrium situation is to take a cutoff based on an estimate of the vortex core size. Our estimation of the vortex core size, detailed in the Appendix, leads to

$$\epsilon_- = \bar{n} \left[ g + B_0 \tilde{\gamma} \left( \frac{B_0 \tilde{\gamma}}{g + B_0 \tilde{\gamma}} \right)^3 \right], \quad (17)$$

where  $B_0 = 0.524$ . The average density  $\bar{n}$  in Eq. (17) will be approximated by its steady state value in the absence of noise (3).

The results of fitting the numerical data for  $d_{\text{BKT}}$  with Eq. (16) are represented by the dashed lines in Figs. 1 and 2 where the determined fitting parameters are  $C_1 = 8.87$ ,  $C_2 = 1.64$ , and  $C_3 = 5.92 \times 10^{-5}$ . The small numerical value of  $C_3$  implies it can actually be set to zero without affecting the quality of the fits. The numerical data in Figs. 1(a) and 2(a) and the main panels in Figs. 1(b) and 2(b) are taken from Ref. [20]. To numerically solve Eq. (2), a finite-difference scheme was used. Specifically, we use periodic boundary conditions for a square of size  $L_x = L_y = 40$  with grid step equal to 0.2. The location of the critical point is determined in the following way: after a long time evolution in the presence of noise, the system was evolved without noise for a short time (few our units of time) before checking for the presence of vortices. This noiseless evolution gives the advantage of cleaning up the density and phase fluctuations while it is too short for the unbound vortex-antivortex pairs to recombine. The propensity for their recombination is reduced [20] with respect to the equilibrium case thanks to outgoing radial currents that provide an effective repulsion between vortices and antivortices.

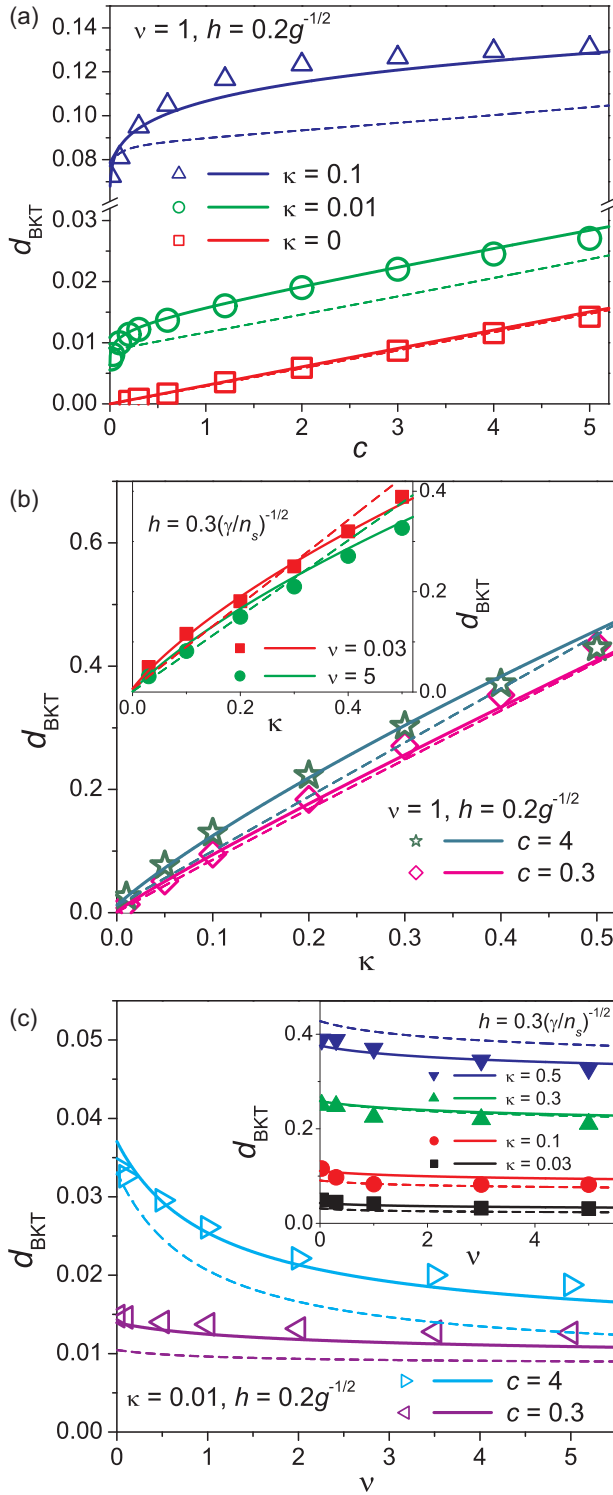


FIG. 1. Numerically (symbols) and semianalytically (lines) determined renormalized critical noise  $d_{\text{BKT}} = D_{\text{BKT}}/n_{\text{BKT}}$  as a function of  $c = \gamma/(2n_s g)$  (a),  $\kappa$  (b), and  $\nu$  (c). The insets in panels (b) and (c) show the dependence of  $d_{\text{BKT}}$  on  $\kappa$  and  $\nu$ , respectively, in the case of  $g = 0$ . The solid and dashed lines correspond to Eqs. (26) and (16), respectively.

To determine the critical noise for the BKT transition,  $D_{\text{BKT}}$ , we use the following criterion. If for a noise intensity  $D$  unbound vortex pairs are present after a noise exposure time  $t_D$  (and hence  $D > D_{\text{BKT}}$ ), while for a certain noise intensity

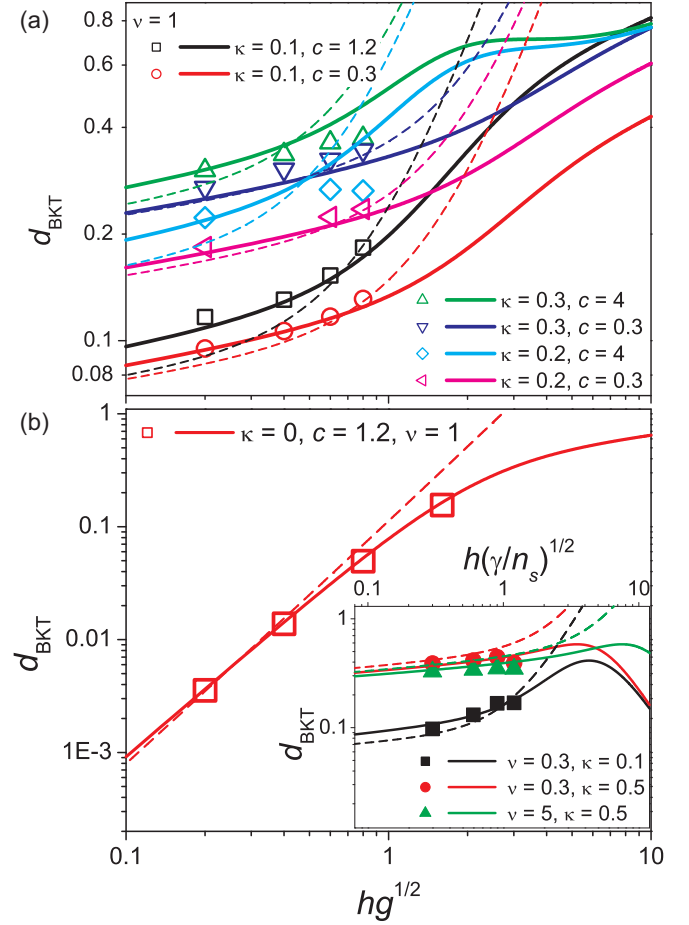


FIG. 2. Numerically (symbols) and semianalytically (lines) determined renormalized critical noise  $d_{\text{BKT}}$  as a function of the grid step at  $\kappa \geq 0.1$  (a) and  $\kappa = 0$  (b) for nonzero  $g$ . Inset in panel (b):  $d_{\text{BKT}}$  as a function of the grid step at  $g = 0$ . The solid and dashed lines correspond to Eqs. (26) and (16), respectively.

$D' < D$  no vortex pairs appear even at noise exposures a few times longer than  $t_D$ , then  $D'$  lies either below  $D_{\text{BKT}}$  or above  $D_{\text{BKT}}$  and closer to  $D_{\text{BKT}}$  than to  $D$ . Therefore, the critical noise intensity can be estimated as  $D_{\text{BKT}} = D' \pm (D - D')$ .

As seen from the comparison between the dashed lines and the symbols in Figs. 1 and 2, Eq. (16) qualitatively reproduces the main trends in the behavior of the numerically determined  $d_{\text{BKT}}(c, \kappa, \nu, h)$  at relatively small grid steps  $h$ , when  $\epsilon_+$  is considerably larger than  $\epsilon_-$ . This qualitative agreement is ensured, in particular, by taking into account the contributions related to density-phase correlation, which are zero in equilibrium systems but play a crucial role for the BKT transition out of equilibrium. At the same time, this simple and transparent heuristic estimate of these contributions does not appear sufficient for a good quantitative description of the numerical results.

## B. Bogoliubov theory with nonlinear correction

In order to obtain a better quantitative description of the numerics for the nonequilibrium BKT transition, we develop below a different approach that leads to a slightly more involved expression. To this purpose, we start from the linear



approximation for the phase fluctuations in the steady state, obtained by solving Eqs. (8)–(10). Inserting  $D/\bar{n}$  from Eq. (8) and  $\langle |\delta n_{\mathbf{k}}/\bar{n}|^2 \rangle$  from Eq. (10) into Eq. (9), we obtain the relation

$$\left[ \epsilon_{\mathbf{k}} + 3g\bar{n} + 2(g^2 + \tilde{\gamma}^2) \frac{\bar{n}^2}{\epsilon_{\mathbf{k}}} \right] \left\langle \frac{\delta\theta_{-\mathbf{k}}\delta n_{\mathbf{k}}}{\bar{n}} \right\rangle = 2\tilde{\gamma}\bar{n}\langle |\delta\theta_{\mathbf{k}}|^2 \rangle. \quad (18)$$

Using Eq. (18), we express  $\langle \delta\theta_{-\mathbf{k}}\delta n_{\mathbf{k}}/\bar{n} \rangle$  through  $\langle |\delta\theta_{\mathbf{k}}|^2 \rangle$  and insert the result into Eq. (8). For the phase fluctuations, this leads to the equation

$$\langle |\delta\theta_{\mathbf{k}}|^2 \rangle = \frac{D}{\bar{n}} f(\epsilon_{\mathbf{k}}), \quad (19)$$

where

$$f(\epsilon) = \frac{1}{2\kappa} \frac{\epsilon + 3\bar{n}g + 2(g^2 + \tilde{\gamma}^2)\bar{n}^2/\epsilon}{(\epsilon + \epsilon_1)(\epsilon + \epsilon_2)} \quad (20)$$

with

$$\epsilon_1 = \bar{n} \left( g + \frac{\tilde{\gamma}}{\kappa} \right), \quad \epsilon_2 = 2\bar{n}g. \quad (21)$$

From Eqs. (19) and (20), one sees that the phase fluctuations are, as expected, proportional to the noise strength  $D$  and decrease as a function of the density  $\bar{n}$  and energy relaxation  $\kappa$ . For what concerns their energy dependence, Eq. (20) shows a  $1/\epsilon$  behavior both at small and large energies. As a consequence, the Fourier transform of phase fluctuations needed to obtain their real space correlations requires the introduction of an infrared cutoff  $\epsilon_-$ , analogous to the treatment in Sec. III A. As a result of Fourier transformation, the local phase variance becomes

$$\langle \delta\theta^2 \rangle = \frac{D}{4\pi\bar{n}} (F + F_-) \quad (22)$$

where

$$\begin{aligned} F = & \int_{\epsilon_-}^{\epsilon_+} f(\epsilon) d\epsilon = \frac{1}{2} \frac{g^2 + \tilde{\gamma}^2}{g(\kappa g + \tilde{\gamma})} \ln \left( \frac{\epsilon_+}{\epsilon_-} \right) \\ & + \frac{\tilde{\gamma}}{\tilde{\gamma} + \kappa g} \left( \frac{1}{2\kappa} + \frac{\kappa\tilde{\gamma}}{\tilde{\gamma} - \kappa g} \right) \ln \left( \frac{\epsilon_+ + \epsilon_1}{\epsilon_- + \epsilon_1} \right) \\ & - \frac{\tilde{\gamma}^2}{2g(\tilde{\gamma} - \kappa g)} \ln \left( \frac{\epsilon_+ + \epsilon_2}{\epsilon_- + \epsilon_2} \right), \end{aligned} \quad (23)$$

where the logarithmic dependence on the lower and upper energy cutoffs is a consequence of the  $1/\epsilon$  behavior of  $f(\epsilon)$  at low and high energies. The term

$$F_- = C_- \epsilon_- f(\epsilon_-) \quad (24)$$

in Eq. (22) approximates the contribution of the integral over  $\epsilon$  from zero to  $\epsilon_-$ , where  $C_-$  is a fitting parameter.

Expression (22), derived with the use of linearized equations for the phase and density fluctuations, is expected to be applicable when these fluctuations are small. As discussed above, at the BKT transition, where both phase and density fluctuations are large, the real space correlator  $\langle \delta\theta\delta n \rangle$  is mainly determined by the contributions of  $k \sim k_+$ . According to Eq. (18), the quantity  $\langle |\delta\theta_{\mathbf{k}}|^2 \rangle$  contains a term that is exactly proportional to  $\langle \delta\theta_{-\mathbf{k}}\delta n_{\mathbf{k}} \rangle$ . This implies that at the BKT

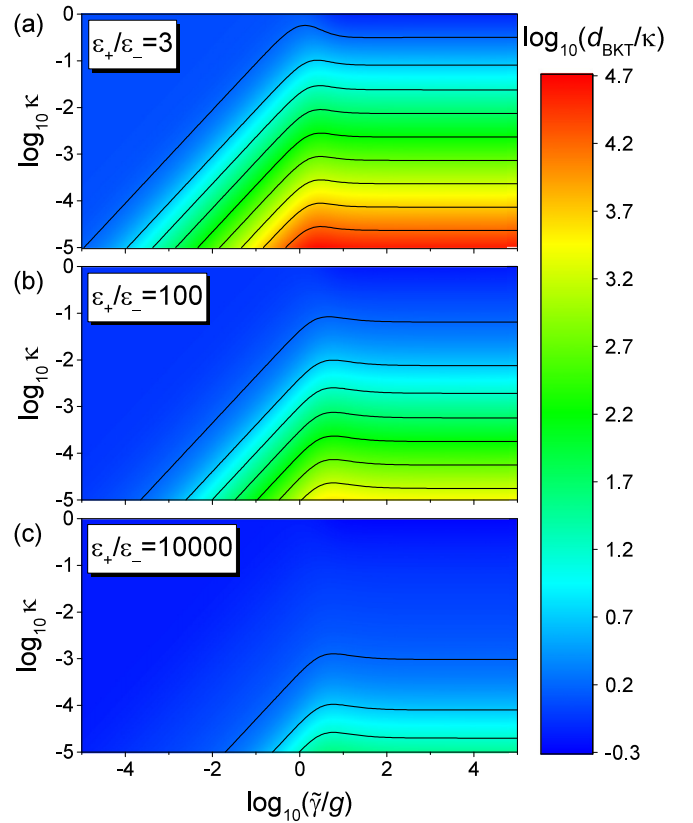


FIG. 3. Renormalized critical noise  $d_{\text{BKT}}/\kappa$ , given by Eq. (26), as a function of  $\tilde{\gamma}/g$  and  $\kappa$  at three different values of  $\epsilon_+/\epsilon_-$ .

transition the expression for the phase fluctuations  $\langle \delta\theta^2 \rangle$ , derived above, needs an additional “nonlinear correction,” which would describe an enhanced contribution of large momenta  $k \sim k_+$  (large energies  $\epsilon \sim \epsilon_+$ ). Here, we approximate this correction by adding to  $F$  the term

$$F_+ = C_+ \epsilon_+ f(\epsilon_+), \quad (25)$$

where  $C_+$  is a fitting parameter. Then at the BKT point we have

$$d_{\text{BKT}} = \langle \delta\theta^2 \rangle_{\text{BKT}} \frac{4\pi}{F + F_- + F_+}, \quad (26)$$

where again we take  $\langle \delta\theta^2 \rangle_{\text{BKT}} = 1/2$ .

Applying Eq. (26) to fit the numerical data for  $d_{\text{BKT}}$ , we obtain for the two fitting parameters  $C_- = 2.24$  and  $C_+ = 7.33$ . As compared to the results of the heuristic approach described in the previous subsection (dashed lines in Figs. 1 and 2), the results corresponding to the more involved and accurate Eq. (26), which are shown by the solid lines in Fig. 1, demonstrate a much better quantitative agreement with the numerically determined  $d_{\text{BKT}}$ .

The semianalytical expression for  $d_{\text{BKT}}$ , given by Eq. (26) together with Eqs. (17), (20), (21), and (23)–(25), can be considered as a function of three independent parameters:  $\tilde{\gamma}/g$ ,  $\kappa$ , and  $\epsilon_+/\epsilon_-$ . In Fig. 3, the renormalized critical noise  $d_{\text{BKT}}/\kappa$ , corresponding to Eq. (26), is plotted for a wide range of the parameters  $\tilde{\gamma}/g$  and  $\kappa$  at three different values of the ratio  $\epsilon_+/\epsilon_-$ .

For small losses and not too small  $\kappa$ , the ratio  $d_{\text{BKT}}/\kappa$  is of order 1, in line with the equilibrium BKT transition where according to the fluctuation-dissipation relation  $D = \kappa T$  [32] and where the critical temperature scales in first approximation as  $T_{\text{BKT}} \sim n$ . In line with our previous studies for polariton condensates [20] and photon condensates [24], we see that the losses stabilize the ordered phase: when  $\tilde{\gamma}$  is increased at fixed  $\kappa$ , the noise required to make the transition to the state with free vortex-antivortex pairs increases. We explained this trend by the reduction of the density fluctuations for increased driving and dissipation [20], that manifests itself through density-phase correlations [24] [see discussions preceding Eqs. (16) and (25)].

In the limit without losses ( $\tilde{\gamma} = 0$ ), our estimate for the critical point reduces to

$$n_{\text{BKT}} = \frac{T_{\text{BKT}}}{2\pi} \left[ \log \left( \frac{1}{mh^2 g n_{\text{BKT}}} \right) + A_1 \right]. \quad (27)$$

Here, we have used that  $T_{\text{BKT}} = D_{\text{BKT}}/\kappa$ , defined  $A_1 = C_+ + C_- + \log(\pi^2/2) \approx 11.2$ , and restored physical units. We can compare this expression with the equilibrium BKT transition for the weakly interacting lattice Bose gas [Eq. (12) in Ref. [12]]:

$$n_{\text{BKT}} = \frac{mT_{\text{BKT}}}{2\pi} \log \frac{A}{mh^2 g T_{\text{BKT}}}, \quad (28)$$

with  $A = 6080$ . This expression can be written as

$$n_{\text{BKT}} = \frac{mT_{\text{BKT}}}{2\pi} \left[ \log \left( \frac{1}{mh^2 g n_{\text{BKT}}} \right) + A_2 \right], \quad (29)$$

with

$$A_2 = \log \left[ \frac{A}{2\pi} \log \left( \frac{A}{m^2 h^2 g T_{\text{BKT}}} \right) \right]. \quad (30)$$

Assuming here  $m^2 h^2 g T_{\text{BKT}} \approx 1$ , one obtains  $A_2 \approx 9.1$ , which is reasonably close to our  $A_1 \approx 11.5$  given the simplicity of our approach and considering that the equilibrium case is actually a somewhat singular limiting case of our model where the gain and losses simultaneously tend to zero.

#### IV. CONCLUSIONS

In this paper, we have developed a semianalytical approach to describe the BKT transition point for driven-dissipative weakly interacting Bose gases. We start from the linearized equations of motion for the density and phase fluctuations and subsequently correct phenomenologically for nonlinearities that are important close to the BKT transition. Our resulting analytical formulas contain some fitting parameters that are fitted to a series of numerical simulations in a wide parameter range. The good fitting of our numerical results indicates the validity of the physical intuition underlying our semianalytical approach and promotes our formulas to a concise summary of the numerical results.

Of course, our numerical results were obtained for a finite size system and we can therefore not settle what will happen for much larger system sizes, where it remains possible that the KPZ nonlinearity may destabilize the algebraically ordered phase [13,17], even though recent numerical work has

shown that KPZ scaling can be witnessed in 2D nonequilibrium condensates without the phase coherence being destabilized by the formation of vortex antivortex pairs [22,23].

#### ACKNOWLEDGMENTS

We thank Iacopo Carusotto for continuous stimulating discussions. V.N.G. was financially supported by Flemish Research Foundation (FWO-Vlaanderen) Grant No. G061820N.

#### APPENDIX: VORTEX DENSITY PROFILE

The vortex core size plays an important role in the BKT physics, because it provides the low energy cutoff in our analytical treatment. In this Appendix, we discuss how the vortex core size depends on the system parameters through an approximate solution of the gGPE, that is shown to compare favorably with the exact numerical solution.

We consider a single-quantum vortex in an infinite 2D condensate. Assuming that the vortex-center position is fixed, the density distribution is circularly symmetric and the order parameter can be written in the cylindrical coordinates  $\rho$  and  $\phi$  as  $\psi = \chi(\rho)e^{-i\phi}$ , so that the condensate density is given by  $n = |\chi|^2$ . Inserting this into the noise-free form of Eq. (2), one has

$$\begin{aligned} \frac{\partial \chi}{\partial t} = (i + \kappa) & \left[ \frac{\partial^2}{\partial \rho^2} + \frac{1}{\rho} \frac{\partial}{\partial \rho} - \frac{1}{\rho^2} - g|\chi|^2 \right. \\ & \left. + \frac{i\gamma}{2n_s} \frac{1 - |\chi|^2}{1 + v|\chi|^2} \right] \chi. \end{aligned} \quad (A1)$$

For analytical estimates it is convenient to represent  $\chi$  as  $\chi(\rho) = \sqrt{\bar{n}}y(\rho)e^{i\theta(\rho)}$ , where the real function  $y(\rho)$  is normalized by 1. Then, taking into account that for a steady state  $\partial y/\partial t = 0$ , while  $\partial \theta/\partial t = -\mu(1 + \kappa^2)$  with  $\mu$ , the chemical potential, one obtains from Eq. (A1) the following two coupled stationary differential equations:

$$\kappa \mu = \frac{\gamma}{2n_s} \frac{1 - \bar{n}y^2}{1 + v\bar{n}y^2} - \frac{1}{\rho y^2} \frac{\partial}{\partial \rho} \left( \rho y^2 \frac{\partial \theta}{\partial \rho} \right), \quad (A2)$$

$$\frac{1}{\rho^2} - \frac{1}{\rho y} \left( \rho \frac{\partial y}{\partial \rho} \right) = \mu - \left( \frac{\partial \theta}{\partial \rho} \right)^2 - g\bar{n}y^2. \quad (A3)$$

In Eq. (A3), the first term corresponds to circulating vortex flows, while the second term in the right hand side is due to outward radial flows from the vortex core [33].

Considering Eq. (A3) in the limit  $\rho \rightarrow \infty$ , one obtains for the chemical potential

$$\mu = \left( \frac{\partial \theta}{\partial \rho} \right)^2 \Big|_{\rho \rightarrow \infty} + g\bar{n}. \quad (A4)$$

Note that in the equilibrium case, when  $\partial \theta/\partial \rho = 0$ , the right hand side of Eq. (A3) is obviously positive. In order to keep it positive also far from equilibrium, one has to assume that  $(\partial \theta/\partial \rho)^2|_{\rho \rightarrow \infty}$  is nonzero. In other words, in the presence of a vortex the chemical potential of a nonequilibrium system should increase.

In the limit  $\rho \rightarrow 0$ , when  $(\partial \theta/\partial \rho)^2$  and  $y^2$  become negligibly small, the general nondivergent solution of the ‘‘reduced’’ equation, resulting from Eq. (A3), is simply  $CJ_1(q\rho)$ , where

$J_1(x)$  is the Bessel function and  $q = \sqrt{\mu}$ . Let us consider the “equilibriumlike” version of Eq. (A3):

$$\frac{1}{\rho^2} - \frac{1}{\rho y} \left( \rho \frac{\partial y}{\partial \rho} \right) = \mu(1 - y^2). \quad (\text{A5})$$

Its solution can be approximated by the normalized by 1 nonoscillating function

$$y_1(\rho) = \frac{1}{J_1(x_*)} J_1 \left( \frac{x}{\sqrt{1 + (x/x_*)^2}} \right), \quad (\text{A6})$$

where  $x = sq\rho$ . The parameters  $s$  and  $x_*$  are determined from the following two requirements.

(i) At small  $\rho$ , the function  $y_1(\rho)$  should coincide with  $CJ_1(q\rho) \approx C[q\rho/2 - (q\rho)^3/16]$ . This leads to  $s = (1 + 4/x_*^2)^{-1/2}$ .

(ii)  $y_1(\rho)$  should satisfy Eq. (A5) in the limit  $\rho \rightarrow \infty$ . In this limit, one has  $1 - y_1(\rho) \propto \rho^{-2}$  and Eq. (A5) becomes

$$\frac{1}{\rho^2} = \mu \frac{x_*^3 J_1'(x_*)}{(sq\rho)^2 J_1(x_*)}, \quad (\text{A7})$$

leading for  $x_*$  to the equation  $J_1'(x_*)(x_*^3 + 4x_*) = J_1(x_*)$ , which gives  $x_* = 1.72$  and, correspondingly,  $s = 0.653$ . As we will see later, in the case of weak nonequilibrium, the function

$$n_1(\rho) = \bar{n}y_1^2(\rho) \quad (\text{A8})$$

describes almost perfectly the vortex density profiles, found in numerical simulations. Moreover, close to the vortex center, this function works quite well even at relatively strong deviations from equilibrium. This is not surprising: close to the vortex center, the vortex circulating-current density, which is proportional to  $1/\rho$ , is much stronger than the radial-current density, so that just the former governs the particle-density suppression.

Let us estimate  $\partial\theta/\partial\rho$ , which determines the radial particle flow. At  $\rho \rightarrow \infty$ , the last term of Eq. (A2) (which is proportional to  $\text{div} j_\rho$ ) vanishes, while  $y$  goes to 1, so that we have

$$\kappa\mu = \frac{\gamma}{2n_s} \frac{1 - \bar{n}}{1 + v\bar{n}}. \quad (\text{A9})$$

Therefore, Eq. (A2) can be rewritten as

$$\frac{1}{\rho y^2} \frac{\partial}{\partial \rho} \left( \rho y^2 \frac{\partial \theta}{\partial \rho} \right) = \tilde{\gamma} \bar{n} \frac{1 - y^2}{1 - p(1 - y^2)} \quad (\text{A10})$$

with  $p = v\bar{n}/(1 + v\bar{n})$ . From Eq. (A10) one obtains

$$\frac{\partial \theta}{\partial \rho} = \frac{\tilde{\gamma} \bar{n}}{sq} Q_p(\rho), \quad (\text{A11})$$

where

$$Q_p(\rho) = \frac{sq}{\rho y^2(\rho)} \int_0^\rho d\rho' \rho' \frac{y^2(\rho')[1 - y^2(\rho')]}{1 - p[1 - y^2(\rho')]} \quad (\text{A12})$$

A finite nonzero value of  $\partial\theta/\partial\rho|_{\rho \rightarrow \infty}$  is possible only if we assume that at  $\rho \rightarrow \infty$

$$n(\rho) = \bar{n}y^2(\rho) \approx \bar{n} \left( 1 - \frac{R}{\rho} \right). \quad (\text{A13})$$

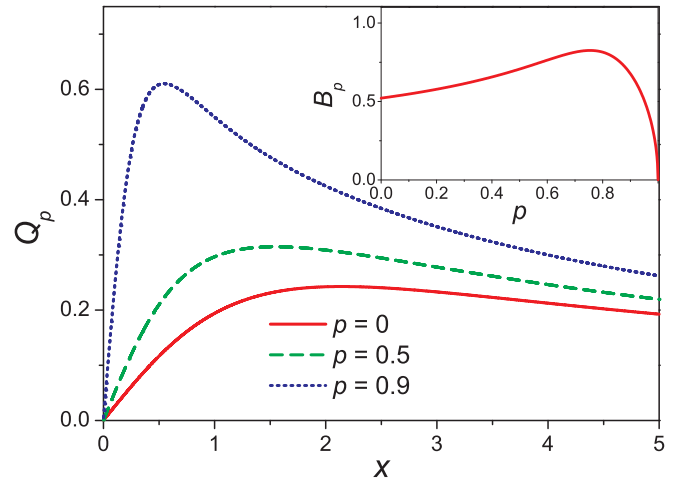


FIG. 4. Function  $Q_p(x)$  with  $y = y_1$  for three different values of  $p$ . Inset: Parameter  $B_p$  as a function of  $p$ .

Then we have from Eqs. (A11) and (A12)

$$\left. \frac{\partial \theta}{\partial \rho} \right|_{\rho \rightarrow \infty} = R\tilde{\gamma}\bar{n}. \quad (\text{A14})$$

At moderate distances from the vortex center, the radial current density increases with  $\rho$ . For sufficiently large  $\tilde{\gamma}$ , the suppressive effect of radial currents on  $y^2$  becomes dominating above certain  $\rho$ , so that the behavior described by Eq. (A13) emerges.

In order to determine the parameter  $R$ , let us consider the crossover between the two regimes, described by Eqs. (A8) and (A13). Let us start with the case of noninteracting particles,  $g = 0$ . The suppressive effect of the radial currents on the particle density is determined by  $(\partial\theta/\partial\rho)^2$ . At  $\rho$  below the crossover point,  $y$  in Eq. (A12) can be approximated by  $y_1$ , so that  $Q_p$  depends on  $\rho$  only through  $x$  (see Fig. 4). It seems natural to expect that the crossover occurs at a distance  $\rho_c$ , where the value of  $Q_p(x)$  is close to its maximum. For simplicity, we will assume that the crossover point  $\rho_c(p)$  just corresponds to the position of this maximum,  $x_m(p)$ , i.e.,  $\rho_c = x_m/(sq)$ . At the crossover point, the solution  $y_1$  for small  $\rho$  should match the solution for large  $\rho$ , described by Eq. (A13). This leads to

$$R = \sqrt{\frac{B_p}{\tilde{\gamma}\bar{n}}} \quad (\text{A15})$$

with

$$B_p = \frac{x_m}{s} [1 - y_1^2(\rho_c)], \quad (\text{A16})$$

where, as seen from Eq. (A6),  $y_1(\rho_c)$  is determined solely by  $x_m(p)$ . The numerically determined dependence of  $B_p$  on  $p$  is shown in the inset of Fig. 4.

We can expect that in the general case, where the interparticle interaction is non-negligible, the crossover occurs when, with increasing  $\rho$ , the density of the radial current becomes comparable with that of the circulating current, so that [see Eq. (A11)]

$$\left( \frac{\tilde{\gamma}\bar{n}}{sq} \right) Q_p(\rho_c) = \frac{C}{\rho_c}. \quad (\text{A17})$$

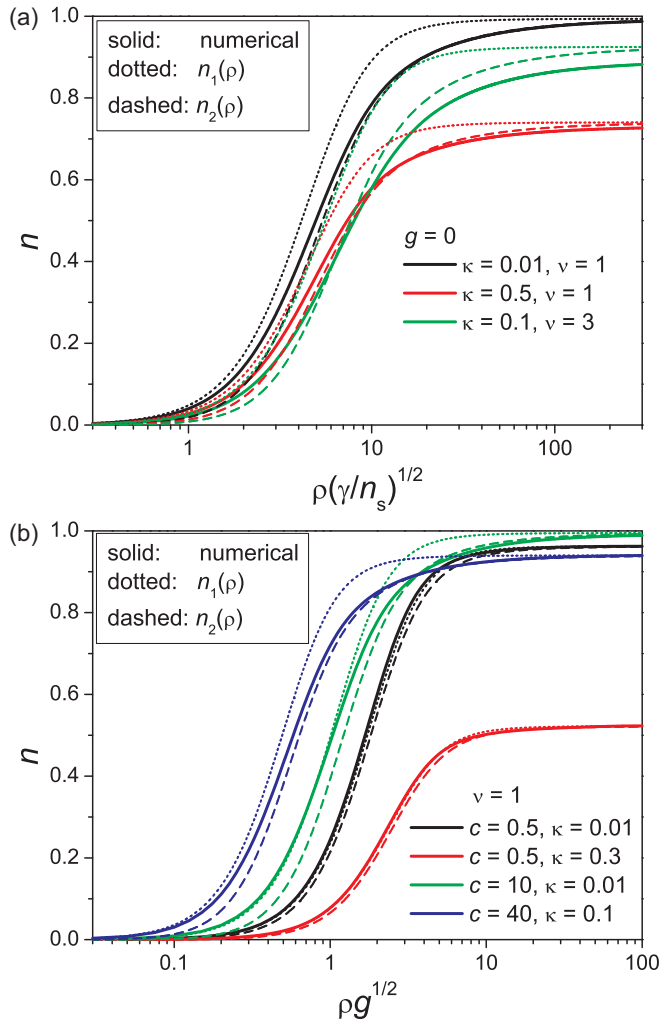


FIG. 5. Numerically (solid lines) and analytically (dotted and dashed lines) calculated density profiles for noninteracting particles (a) and three finite values of the parameter  $c = \gamma/(2n_s g)$  (b) at different  $\nu$  and  $\kappa$ .

Obviously, with increasing  $g$  the suppressive effect of radial currents on the particle density becomes relatively weaker. Therefore,  $R$  should decrease with increasing  $g$  or decreasing  $\gamma$  ( $R = 0$  at  $\gamma = 0$ ). This means that at non-negligible  $g$  the matching condition at the crossover point,  $R/\rho_c = 1 - y_1^2(x_c)$ , corresponds to a rather small value of  $1 - y_1^2(x_c)$ , which can be approximated [see Eqs. (A6) and (A7)] by  $1/(q\rho_c)^2$ . Then the matching condition becomes  $1/\rho_c = Rq^2$ . Inserting this

into Eq. (A17), we obtain

$$R = \frac{Q_p(\rho_c) (\tilde{\gamma}\bar{n})}{sC q^3}. \quad (\text{A18})$$

For simplicity, in the denominator  $q^3$  we approximate  $R$  by the value given by Eq. (A15). The constant  $C$  is determined by requiring that in the limit  $g \rightarrow 0$  the  $R$ , given by Eq. (A18), fits Eq. (A15). Then for  $R$  we finally have

$$R = \sqrt{\frac{B_p}{\tilde{\gamma}\bar{n}}} \left( \frac{B_p \tilde{\gamma}}{g + B_p \tilde{\gamma}} \right)^{3/2}. \quad (\text{A19})$$

From Eqs. (A4) and (A14) with (A19), we obtain the relation

$$\mu = \bar{n} \left[ g + B_p \tilde{\gamma} \left( \frac{B_p \tilde{\gamma}}{g + B_p \tilde{\gamma}} \right)^3 \right]. \quad (\text{A20})$$

Equations (A20) and (A9) completely define the chemical potential  $\mu$  and average density  $\bar{n}$ , which, together with the parameter  $R$  given by Eq. (A19), enter the density distributions (A8) and (A13) at small and large  $\rho$ , respectively. As a “smooth interpolation” between these distributions, we introduce the function

$$n_2(\rho) = \frac{1}{1 + R/\rho} n_1(\rho). \quad (\text{A21})$$

Obviously, this function can somewhat underestimate  $n$  at  $\rho \sim R$ , close to the “bottom” of the vortex core. Apart from this, as seen from Fig. 5(a), at  $g = 0$  the function  $n_2(\rho)$  approximates rather well the vortex shape, found by solving Eq. (A6) numerically, although the analytical value of  $\bar{n}$  appears not quite accurate for (experimentally less relevant) large  $\kappa$  (red curves) and large  $\nu$  (green curves). For strongly interacting particles and/or for weak deviations from equilibrium, when the parameter  $c = \gamma/(2n_s g)$  is smaller than 1, the numerical results are almost perfectly described by the equilibriumlike profile  $n_1(\rho)$  [see the black and red curves in Fig. 5(b)]. For  $c > 1$ , the numerically determined  $n(\rho)$  at large  $\rho$  is well approximated by  $n_2(\rho)$  [see the green and blue curves in Fig. 5(b)].

The obtained results show that the  $\mu$  given by Eq. (A20) ( $q^{-1} = 1/\sqrt{\mu}$ ) adequately describes the chemical potential (vortex core size) in the systems under consideration. This implies that Eq. (A20) can provide a suitable estimate for the lower energy cutoff  $\epsilon_-$ . Since for experimentally relevant  $p < 0.9$  the parameter  $B_p$  relatively weakly depends on  $p$ , in this estimate, for simplicity, we replace  $B_p$  with  $B_0 = 0.524$ .

[1] J. Bloch, I. Carusotto, and M. Wouters, *Nat. Rev. Phys.* **4**, 470 (2022).  
 [2] I. Carusotto, A. A. Houck, A. J. Kollár, P. Roushan, D. I. Schuster, and J. Simon, *Nat. Phys.* **16**, 268 (2020).  
 [3] R. Labouvie, B. Santra, S. Heun, and H. Ott, *Phys. Rev. Lett.* **116**, 235302 (2016).  
 [4] M. Van Regemortel, Z.-P. Cian, A. Seif, H. Dehghani, and M. Hafezi, *Phys. Rev. Lett.* **126**, 123604 (2021).

[5] S. Diehl, A. Micheli, A. Kantian, B. Kraus, H. Büchler, and P. Zoller, *Nat. Phys.* **4**, 878 (2008).  
 [6] M. Wouters and I. Carusotto, *Phys. Rev. B* **74**, 245316 (2006).  
 [7] A. Chiochetta and I. Carusotto, *Europhys. Lett.* **102**, 67007 (2013).  
 [8] V. L. Berezinskii, *Sov. Phys. JETP* **32**, 493 (1971).  
 [9] J. M. Kosterlitz and D. J. Thouless, *J. Phys. C* **6**, 1181 (1973).  
 [10] D. J. Bishop and J. D. Reppy, *Phys. Rev. Lett.* **40**, 1727 (1978).



- [11] Z. Hadzibabic, P. Krüger, M. Cheneau, B. Battelier, and J. Dalibard, *Nature (London)* **441**, 1118 (2006).
- [12] N. Prokof'ev, O. Ruebenacker, and B. Svistunov, *Phys. Rev. Lett.* **87**, 270402 (2001).
- [13] G. Wachtel, L. M. Sieberer, S. Diehl, and E. Altman, *Phys. Rev. B* **94**, 104520 (2016).
- [14] K. Ji, V. N. Gladilin, and M. Wouters, *Phys. Rev. B* **91**, 045301 (2015).
- [15] V. N. Gladilin, K. Ji, and M. Wouters, *Phys. Rev. A* **90**, 023615 (2014).
- [16] Q. Fontaine, D. Squizzato, F. Baboux, I. Amelio, A. Lemaître, M. Morassi, I. Sagnes, L. Le Gratiet, A. Harouri, M. Wouters *et al.*, *Nature (London)* **608**, 687 (2022).
- [17] E. Altman, L. M. Sieberer, L. Chen, S. Diehl, and J. Toner, *Phys. Rev. X* **5**, 011017 (2015).
- [18] G. Dagvadorj, J. M. Fellows, S. Matyjaśkiewicz, F. M. Marchetti, I. Carusotto, and M. H. Szymańska, *Phys. Rev. X* **5**, 041028 (2015).
- [19] D. Caputo, D. Ballarini, G. Dagvadorj, C. S. Muñoz, M. De Giorgi, L. Dominici, K. West, L. N. Pfeiffer, G. Gigli, F. P. Laussy *et al.*, *Nat. Mater.* **17**, 145 (2018).
- [20] V. N. Gladilin and M. Wouters, *Phys. Rev. B* **100**, 214506 (2019).
- [21] G. Dagvadorj, P. Comaron, and M. Szymanska, *Phys. Rev. Lett.* **130**, 136001 (2023).
- [22] Q. Mei, K. Ji, and M. Wouters, *Phys. Rev. B* **103**, 045302 (2021).
- [23] K. Deligiannis, Q. Fontaine, D. Squizzato, M. Richard, S. Ravets, J. Bloch, A. Minguzzi, and L. Canet, *Phys. Rev. Res.* **4**, 043207 (2022).
- [24] V. N. Gladilin and M. Wouters, *Phys. Rev. A* **104**, 043516 (2021).
- [25] V. N. Gladilin and M. Wouters, *Phys. Rev. Lett.* **125**, 215301 (2020).
- [26] M. Wouters and V. Savona, *Phys. Rev. B* **79**, 165302 (2009).
- [27] M. H. Szymanska, J. Keeling, and P. B. Littlewood, *Phys. Rev. B* **75**, 195331 (2007).
- [28] L. M. Sieberer, M. Buchhold, and S. Diehl, *Rep. Prog. Phys.* **79**, 096001 (2016).
- [29] I. Carusotto and C. Ciuti, *Rev. Mod. Phys.* **85**, 299 (2013).
- [30] M. Wouters, *New J. Phys.* **14**, 075020 (2012).
- [31] K. Jacobs, *Stochastic Processes for Physicists: Understanding Noisy Systems* (Cambridge University, New York, 2010).
- [32] P. C. Hohenberg and B. I. Halperin, *Rev. Mod. Phys.* **49**, 435 (1977).
- [33] V. N. Gladilin and M. Wouters, *New J. Phys.* **19**, 105005 (2017).